Journal of Clinical and Translational Hepatology **2022**
DOI: 10.14218/JCTH.2022.00048

Original Article

MgIG Attenuates Oxaliplatin-induced Hepatotoxicity through Suppression of Connexin 43 in Hepatic Stellate Cells

Yuzhu Cao[1], Yawen Xia[1], Yufei Wang[1], Hang Shi[1], Yuanyuan Wu[1,2*] and Yin Lu[1,2*]

[1]School of Pharmacy, Jiangsu Key Laboratory for Pharmacology and Safety Evaluation of Chinese Materia Medica, Nanjing University of Chinese Medicine, Nanjing, Jiangsu, China; [2]Jiangsu Collaborative Innovation Center of Traditional Chinese Medicine Prevention and Treatment of Tumor, Nanjing University of Chinese Medicine, Nanjing, Jiangsu, China

Received: 30 January 2022 | **Revised:** 24 July 2022 | **Accepted:** 16 August 2022 | **Published:** 5 December 2022

Abstract

Background and Aims: Oxaliplatin is widely used in cancer chemotherapy with adverse effects such as liver toxicity. Magnesium isoglycyrrhizinate (MgIG) has hepatoprotective effects, but the underlying mechanism remains elusive. The study's aim was to investigate the mechanism underlying the hepatoprotective effects of MgIG against oxaliplatin-induced liver injury. ***Methods:*** A xenografted colorectal cancer mouse model was established with MC38 cells. Mice were given oxaliplatin (6 mg/kg/week) for 5 weeks to mimic oxaliplatin-induced liver injury *in vivo*. LX-2 human hepatic stellate cell s(HSCs) were employed for *in vitro* studies. Serological tests, hematoxylin and eosin staining, oil red O staining and transmission electron microscopy were used for histopathological examinations. Real-time PCR, western blotting, immunofluorescence and immunohistochemical staining were used to determine Cx43 mRNA or protein levels. Flow cytometry was used to assay reactive oxygen species (ROS) and mitochondrial membrane. Short hairpin RNA targeting Cx43 was lentivirally transduced in LX-2 cells. Ultra-high performance liquid chromatography-tandem mass spectrometry was used to determine MgIG and metabolite concentration. ***Results:*** MgIG (40 mg/kg/day) treatment significantly reduced serum aspartate transaminase (AST) and alanine transaminase (ALT) levels in the mouse model, and alleviated liver pathological changes, including necrosis, sinusoidal expansion, mitochondrial damage, and fibrosis. MgIG reduced the abnormal expression of Cx43 in the mitochondria and nuclei of HSCs. MgIG inhibited the activation of HSCs via reducing ROS generation, mitochondrial dysfunction, and N-cadherin transcription. MgIG's inhibition of HSCs activation was abolished after knockdown of Cx43 in LX-2 cells. ***Conclusions:*** Cx43 mediated MgIG's hepatoprotective effects against oxaliplatin-induced toxicity.

Keywords: Magnesium isoglycyrrhizinate; Hepatoprotective; 18 α-Glycyrrhetinic acid; Mitochondrial dysfunction; Hepatic stellate cell; Connexin 43.

Abbreviations: ALT, alanine transaminase; AST, aspartate transaminase; Cx43, connexin 43; HSC, hepatic stellate cell; MgIG, magnesium isoglycyrrhizinate; PBS, phosphate buffered saline; ROS, reactive oxygen species.

[*]**Correspondence to:** Yuanyuan Wu and Yin Lu, School of Pharmacy, Jiangsu Key Laboratory for Pharmacology and Safety Evaluation of Chinese Materia Medica, Nanjing University of Chinese Medicine, Nanjing, Jiangsu 210023, China. ORCID: https://orcid.org/0000-0001-6231-2315 (YW) and https://orcid.org/0000-0003-2063-8485 (YL). Tel: +86-25-85811237 (YW) and +86-25-85811239 (YL), Fax: +86-25-85811237, E-mail: ywu@njucm.edu.cn (YW) and luyingreen@njucm.edu.cn (YL)

Citation of this article: Cao Y, Xia Y, Wang Y, Shi H, Wu Y, Lu Y. MgIG Attenuates Oxaliplatin-induced Hepatotoxicity through Suppression of Connexin 43 in Hepatic Stellate Cells. J Clin Transl Hepatol 2022. doi: 10.14218/JCTH.2022.00048.

Introduction

Oxaliplatin is widely used for the treatment of colorectal cancer.[1,2] However, studies have shown that systemic chemotherapy containing oxaliplatin causes hepatic sinusoidal dilatation in up to 78% of patients.[3] In the liver, oxaliplatin can also cause hepatic stellate cell (HSC) activation and liver endothelial cell apoptosis.[4–6] In addition, increased generation of reactive oxygen species (ROS) associated with mitochondrial dysfunction is a primary cause of oxaliplatin toxicity in the liver.[7,8] Protecting the liver while treating the tumor with oxaliplatin is the key to successful treatment.[9]

Clinical studies have revealed that prophylactic administration of magnesium isoglycyrrhizinate (MgIG) significantly reduced the incidence of liver injury induced by oxaliplatin.[7,10,11] MgIG is a novel α-isomer compound synthesized from 18 β-glycyrrhizic acid by isomerization and salification, and has been used in the treatment of chronic hepatitis. Moreover, MgIG protects against liver injury induced by various chemotherapy drugs, including oxaliplatin, paclitaxel, and epirubicin.[8] Studies of MgIG's metabolism showed that it was mainly distributed in the liver tissue through liver and intestine circulation.[12] The current understanding of MgIG's hepatoprotection includes preventing or reducing hepatotoxicity by scavenging free radicals induced by toxins, such as concanavalin A and cyclophosphamide.[13,14]

Connexin 43 (Cx43) is an important gap junction protein that allows intercellular communication between adjacent cells. In addition to its canonical role at the plasma membrane, connexin can produce small fragments that are present in different cellular compartments, including the nucleus, and act as transcriptional factors to regulate gene expression.[15] Cx43 protects the liver from acute-on-chronic liver failure, cirrhosis, and acetaminophen hepatotoxicity,[2,16] but the effectiveness of Cx43 in oxaliplatin-based chemotherapy is controversial. In *in vitro* cell models, Cx43 enhanced oxaliplatin cytotoxicity and oxaliplatin inhibited Cx43 expression.[17] Studies have shown that Cx43 mediates the development of resistance to oxaliplatin-based chemothera-

peutic agents in colorectal cancer.[18] Zou *et al*.[8] have described the hepatoprotective effects of MgIG in an oxaliplatin-induced model of liver injury, which were associated with effects of MgIG on oxidative stress and the proinflammatory cytokine interleukin (IL)-6. The mechanistic link between Cx43 and MgIG in oxaliplatin-induced liver injury remains elusive.

In this study, we established a mouse model of oxaliplatin-induced liver injury to demonstrate HSC activation in oxaliplatin-induced liver injury. The hepatoprotective effects of MgIG were associated with inhibition of HSC activation mediated by metabolite of MgIG on mitochondria Cx43. This study describes the molecular mechanism underlying the hepatoprotective activity of MgIG beyond the oxidative stress pathway and provides evidence in support of Cx43 as a potential therapeutic target in oxaliplatin-induced liver injury.

Methods

Chemicals and reagents

MgIG (Lot: 00215027, purity > 98%) was provided by Chia Tai Tianqing Pharmaceutical Group Co., Ltd. (Lianyungang, Jiangsu Province, P. R. China**)** and oxaliplatin (Item no. O124003, CAS No. 61825-94-3) was provided by Shanghai Aladdin Biochemical Technology Co. Ltd. (Shanghai, China). Lipopolysaccharide (LPS) was purchased from Sigma (Sigma, St. Louis, MO, USA).

Mice and xenograft model establishment

The mice were housed in the specific pathogen-free barrier facility at Nanjing University of Chinese Medicine. Ten-week-old female C57BL/6 mice were obtained from Beijing Vital River Laboratory Animal Technology Co., Ltd (Beijing, China). The tumor-bearing model was established by subcutaneously inoculating 5×10^5 MC-38 cells into the right flank of the mice. MC-38 cells were derived from chemically induced colon cancer tissue of C57BL/6 female mice.[19] Therefore, female mice were used in this study. To determine the protective effectiveness of MgIG, C57BL/6 mice were treated by intraperitoneal injection of MgIG 40 mg/kg once daily followed 1 h later by oxaliplatin 6 mg/kg) for 5 weeks. After 5 weeks, the mice were fasted 12 h and euthanized for blood collection and harvesting liver and tumor tissue.

Cell lines and treatment

The MC-38 colon cancer cell line was kindly provided by Professor Zhang Xiaohong (School of Medicine, Ningbo University, China), and the immortalized LX-2 HSC line was gifted by Professor Zheng Shizhong (Nanjing University of Chinese Medicine). MC-38 and LX-2 were cultured in Dulbecco's modified eagle medium containing 10% fetal calf serum, 100 U/mL penicillin, 100 μg/mL streptomycin, and 2 mM L-glutamine. LX-2 cells were treated with 2 μg/mL oxaliplatin for 24 h, and 40 μg/mL MgIG was given 1 h before oxaliplatin. Cx43-knockdown short hairpin (sh)RNA constructs were lentivirally packaged and transduced into LX-2 cells according to the manufacturer's instructions (Genepharma, Shanghai, China). The target region sequences were CCAAACTGATGGTGTCAAT. Lentivirally transduced cells were selected with complete medium containing 1 μg/mL puromycin (Sigma).

Determination of MgIG and 18 α-glycyrrhetinic acid in liver tissue

MgIG was administered to mice intraperitoneally at a dose of 40 mg/kg/day. After 5 weeks, the mice were euthanized. Mitochondria and nuclei from mouse liver were collected with tissue mitochondria isolation and nuclear and cytoplasmic protein extraction kits (Beyotime Biotechnology, Shanghai, China). The protein supernatant was processed and determined as previously described.[20] Mitochondria and nuclei were collected from LX-2 cells with cell mitochondria isolation and nuclear and cytoplasmic protein extraction kits (Beyotime Biotechnology, Shanghai, China). MgIG and 18 α-glycyrrhetinic acid were assayed by ultra-high performance liquid chromatography-tandem mass spectrometry (UPLC-MS/MS; Acquity UPLC and Xevo TQ tandem quadrupole mass spectrometer (Waters Corporation, Milford, MA, USA).[20] Separation was performed on Shim-pack XP-ODS II columns (75 mm×2.0 mm, 2.2 μm). The mobile phase was 0.1% formic acid in water as phase A and acetonitrile as phase B. Gradient elution was performed as: initial to 35% B (0–0.5 m), 35% to 72% B (0.5–1.0 m), 72% B (1.0–1.6 m), 72–80% B (1.6–3.5 m), 80% B (3.5–3.7 m), 80–35% B (3.7–3.9 m), and stop at 5 m. The flow rate was 0.4 mL/m and the column temperature was 40°C. The retention times were 1.66 m for MgIG and 3.00 m for 18 α-glycyrrhetinic acid. The mass spectrometer was equipped with an electrospray ionization source. The source parameters were a desolvation gas flow of 1,000 L/h at a temperature of 550°C, a cone gas flow of 50 L/h, and a source temperature of 150°C. The capillary voltage was 3,000 V. Analyte detection was performed by multiple reaction monitoring (MRM). The cone voltage setting depended on the specific MRM for each compound. Data was collected in MRM mode by simultaneously screening parent and daughter ions. Dwell time was automatically set by the software. MgIG and 18 α-glycyrrhetinic acid standards were obtained from Chia Tai Tianqing Pharmaceutical Group Co., Ltd.. The standard curve was calculated as $y=2E-07x + 8E-06$, $R^2=0.9999$ (MgIG); $y=2E-05x - 0.003$, $R^2=0.9998$ (18 α-glycyrrhetinic acid). Quantification of the target compounds concentrations was based on the peak areas of the sample and the standards.

Histopathology and immunohistochemical (IHC) staining

Small pieces of liver tissue from each study group were fixed in 4% paraformaldehyde for 24–48 h and embedded in paraffin. The blocks were cut into 3 μm slices, processed for hematoxylin-eosin (H&E) and IHC staining using standard protocols. The antibodies used for IHC were rabbit anti-Cx43 (Cell Signaling Technology, Danvers, MA, USA; #3512S, 1:500) and rabbit anti-α-SMA (Proteintech, Singapore; # 14395-1-AP, 1:200) as previously described. The percentage of Cx43-positive cells was determined as the ratio of diaminobenzidine-stained / nuclear hematoxylin-stained cells. Staining results were captured with a Mantra quantitative pathology workstation (Mantra; PerkinElmer Inc., Hopkinton, MA, USA) and quantified by ImageJ (Bethesda, MD, USA).[21]

Immunofluorescence

Tissue sections of 3 μm thickness were baked in oven at 62°C for 6 h before dewaxing and rehydration. The slides were washed with phosphate buffered saline (PBS) three times before and after heat-induced antigen retrieval. LX-2 cells seeded on coverslips were fixed in methanol for 20 m and permeabilized with 0.1% Triton X-100 (Genview Life Scientific Inc, Tampa, FL, USA) for more than 10 m. Endogenous peroxidases were blocked with 3% H_2O_2 for 20 m. Nonspecific staining was preblocked with PBS containing 2.5% bovine serum albumin. The primary antibodies were rabbit anti-Cx43

(Cell Signaling Technology; Danvers, Massachusetts, USA, #3512S, 1:500), rabbit anti-TOM20 (Proteintech; #11802-1-AP, 1:1,000), rabbit anti-α-SMA (Proteintech; #14395-1-AP, 1:200) or chicken anti-glial fibrillary acidic protein (GFAP) (Abcam, Cambridge, UK; #ab4674) at 4°C overnight. The secondary antibodies were goat anti-rabbit IgG (Santa Cruz Biotechnology, Dallas, TX, USA; 1:200), Alexa Fluor 594 goat anti-mouse IgG (H+L); Proteintech; #SA00006-3) or Goat anti-chicken IgY H+L (Alexa Fluor 647; Abcam; ab150171) or Hoechst 33342 (Beyotime Biotechnology, Shanghai, China) for 10 m. Stained sections were scanned by fluorescence optical microscopy (Mantra; PerkinElmer).

Transmission electron microscopy

Fresh liver samples were fixed in 2.5% glutaraldehyde for no more than 2 m and kept at 4°C. Tissue was post-fixed in 1.5% osmic acid for about 1 h and washed with 0.1 M PBS and then dehydrated in a 50–100% alcohol series, transferred to pure acetone, embedded, sliced into 70 nm sections, and stained with uranyl acetate and lead citrate. The sections were observed with a Hitachi H-7650 electron microscope.

Western blot assay

Protein extracts of liver tissues were loaded on sodium dodecyl sulfate–polyacrylamide gels and transferred to polyvinylidene difluoride membranes (EMD Millipore, Burlington, MA, USA) after electrophoresis. Protein concentration was determined with a bicinchoninic acid protein assay kit (Beyotime Biotechnology, Shanghai, China). The proteins were marked with anti-Connexin 43 (Cell Signaling Technology; Danvers, Massachusetts, USA, #3512S, 1:1,000), N-cadherin (Cell Signaling Technology; Danvers, Massachusetts, USA, #13116S, 1:1,000), GAPDH (Cell Signaling Technology; Danvers, Massachusetts, USA, #2118s, 1:1,000), TOM20 (Proteintech; Wuhan, China, #11802-1-AP, 1:1,000), or collagen I (Abcam; Cambridge, CB2 0AX, UK, #ab117119,1:1,000). Enhanced chemiluminescence was used for final detection. Secondary antibodies were used at a dilution of 1:10,000. Gels were imaged using a Bio-Spectrum Gel Imaging System (Bio-Rad Laboratories, Hercules, CA, USA), and band intensity was measured with Photoshop CS6 software (Adobe, San Jose, CA, USA). Cx43 protein bands were normalized to TOM2. Mitochondria from LX-2 cells were collected with a mitochondria isolation kit (Beyotime Biotechnology, Shanghai, China).

Real-time PCR

Total RNA was extracted from LX-2 cells after MgIG treatment using RNAiso Plus (Takara, Dalian, China) according to the manufacturer's instructions. Total RNA was reverse transcribed with Fast Quant RT kits (Tiangen Biotech Co., Ltd, Beijing, China) and quantified by SYBR green PCR Master Mix (Thermo Fisher Scientific, Waltham, MA, USA). Reactions were run on a 7500 Fast Real-Time PCR System (Applied Biosystems Inc., Waltham, MA, USA). The oligonucleotide sequences of the primers (Sangon Biotech, Shanghai, China) were 5′-CAATCTCTCATGTGCGCTTCT-3′ (sense) and 5′-GGCAACCTTGAGTTCTTCCTCT-3′ (antisense) for *Cx43(GJA1)* and 5′-CTTCTTTTGCGTCGCCAGCCGA-3′ (sense) and 5′-ACCAGGCGCCCAATACGACCAA-3′ (antisense) for glyceraldehyde-3-phosphate dehydrogenase (*GAPDH*).

Oil red O staining

Liver tissue sections or LX-2 cell-seeded coverslips were fixed with formaldehyde-calcium solution for 10 m and soaked in 60% isopropanol after washing with distilled water. After 10 m of staining with Oil Red O solution (Solarbio, Beijing, China), differentiation with 60% isopropanol, and washing with distilled water, the preparations were counterstained with Mayer's hematoxylin. Tissue sections and cells were imaged with a microscope and digital camera (Mantra; PerkinElmer). Evaluation and quantification were carried out as previously described.[22,23]

Measurement of ROS and mitochondrial membrane potential

ROS levels and the mitochondrial membrane potential of LX-2 cells were measured with commercially available kits (Beyotime Biotechnology, Shanghai, China) and Mitochondrial Membrane Potential Assay Kit were used (Beyotime Biotechnology, Shanghai, China). LX-2 cells were plated in 6-well plates at a density of 10^5/well, treated with 2 μg/mL oxaliplatin for 24 h, with 40 μg/mL MgIG given 1 h in advance of oxaliplatin. For ROS determination, dichloro-dihydro-fluorescein diacetate (DCFH-DA) was diluted with basal medium to a final concentration of 10 μmol/L. Cells were collected and resuspended in diluted DCFH-DA at a concentration of 1×10^6/mL, and incubated at 37°C for 20 m. The probe and cells were thoroughly mixed. The cells were washed three times with serum-free cell culture medium, after digestion, and assayed by flow cytometry (Accuri C6; BD Biosciences, Franklin Lakes, NJ, USA). To measure mitochondrial membrane potential, cells were resuspended in 0.5 mL of culture medium and 0.5 mL of JC-1 staining working solution. The cells and the probes were incubated 20 m at 37°C and then centrifuged at 600 g for 4 m. The precipitated cells were washed twice with 1× PBS, resuspended in JC-1 staining buffer (1×), and assayed by flow cytometry (Accuri C6; BD Biosciences).

Statistical analysis

Statistical analysis was conducted with GraphPad software (GraphPad Software Inc., La Jolla, CA, USA). All results were obtained from independent triplicate assays unless otherwise indicated and were reported as means ± standard deviation (SD). Multiple group comparisons were done by one-way analysis of variance. $P<0.05$ was considered statistically significant.

Results

MgIG alleviates hepatotoxicity induced by oxaliplatin in tumor-bearing mice

MgIG 40 mg/kg/day in mice was determined to be equivalent to a clinical dose in humans. Compared to the vehicle group, robust increase was found in serum AST and ALT in the oxaliplatin treatment group ($p<0.01$ and $p<0.001$, respectively). Prophylactic administration of MgIG before treatment with oxaliplatin showed significant attenuation in AST and ALT compared with oxaliplatin-treated animals (Fig. 1, $p<0.01$ and $p<0.001$, respectively). No significant differences in AST and ALT level were observed between the control and MgIG-treatment groups (Fig. 1A, B). The inhibitory effect of oxaliplatin on tumor size was not affected by MgIG (Fig. 1C). Histological analysis of liver tissue in vehicle and MgIG groups showed normal patterns. Liver tissue in the oxaliplatin treatment group demonstrated infiltration of inflammatory cells, loss of cellular integrity, and necrosis. Prophylactic administration with MgIG before oxaliplatin markedly suppressed the histological anomalies compared with the oxaliplatin group (Fig. 1D). Transmission electron micrographs of liver tissue in the oxaliplatin treatment group showed significant lysosome

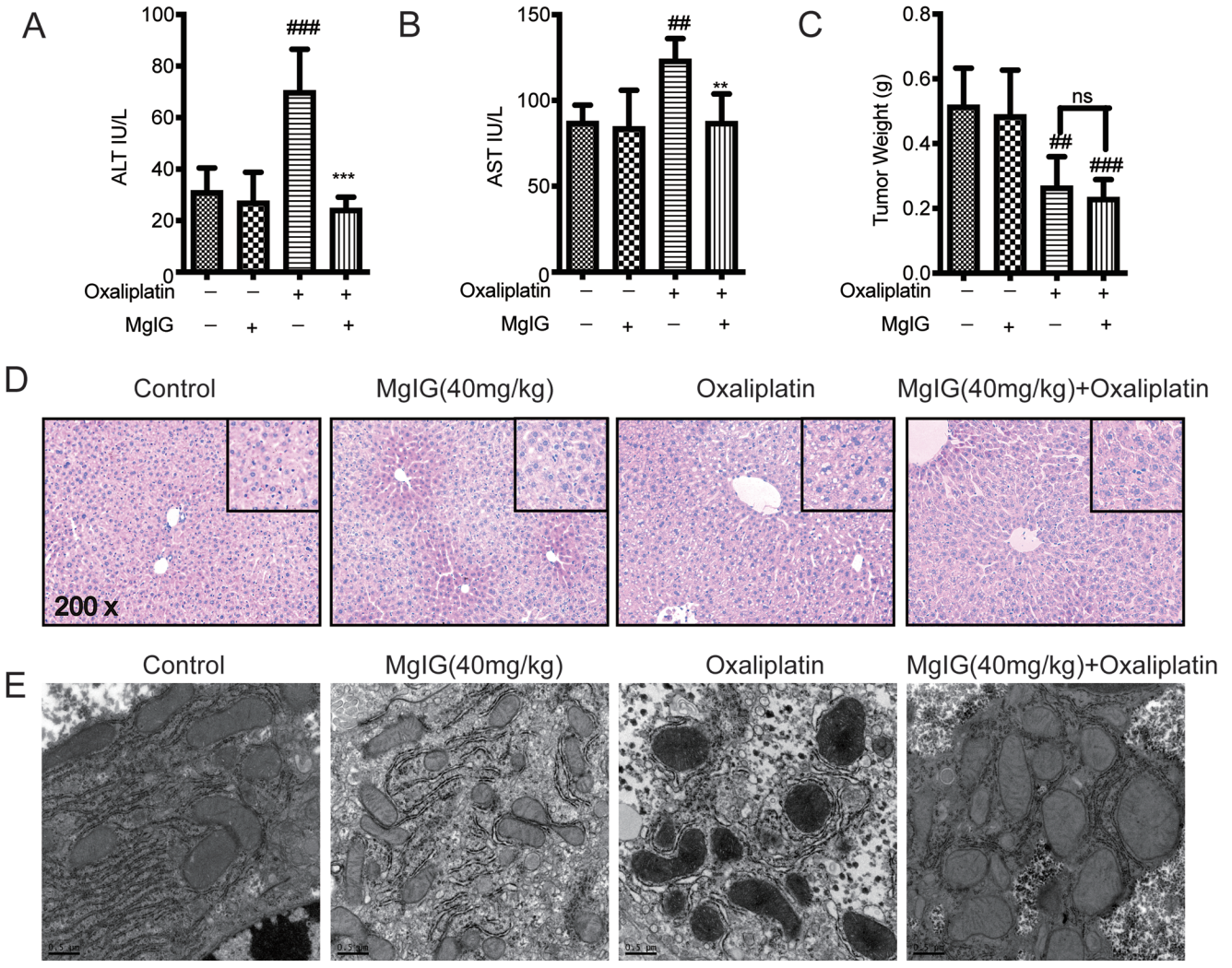

Fig. 1. Daily treatment with MgIG (40 mg/kg) for 5 weeks protected tumor-bearing mice from oxaliplatin-induced hepatotoxicity. Mice were xenografted with MC38 murine colon carcinoma cells and injected with oxaliplatin (6 mg/kg) once a week. Livers, sera, and tumors were obtained from the mice after 5 weeks of treatment. (A, B) Serum ALT and AST levels were measured. (C) Tumors were weighed at the endpoint. (D) Representative H&E staining of liver tissue (original magnification ×200). (E) Representative transmission electron micrographs of liver (0.5 μm in diameter). Compared with the untreated group: $^{\#}p<0.05$, $^{\#\#}p<0.01$, $^{\#\#\#}p<0.001$; Compared with the oxaliplatin-treated group: $^{*}p<0.05$, $^{**}p<0.01$, $^{***}p<0.001$. Six mice per group. ALT, alanine transaminase; AST, aspartate transaminase; MgIG, magnesium isoglycyrrhizinate.

aggregation and mitochondrial damage. MgIG pretreatment markedly ameliorated these phenomena (Fig. 1E).

Distribution of MgIG and its metabolite 18 α-glycyrrhetinic acid in liver tissue

The distribution of MgIG and its metabolites 18-α-glycyrrhetinic acid (Fig. 2A, B) in liver cell nuclei, mitochondria, and the cytoplasm external to the mitochondria was were determined by UPLC-MS/MS. Normalization against protein concentration, showed that mitochondria had higher concentrations of MgIG and 18-α-glycyrrhetinic acid than the nuclei, indicating accumulation of the compounds in mitochondria in the liver (Fig. 2C, D). Next, we explored potential targets that mediated MgIG and its metabolite's protective function in liver mitochondria. Cx43 is a protein in gap junctions, which are involved in liver damage caused by various drugs, as well as diseases such as liver fibrosis and cirrhosis.[24] Therefore, we determined whether Cx43 expression was altered in the livers of mice treated with oxaliplatin or MgIG. The results showed that oxaliplatin induced the expression of Cx43 in the liver tissue of tumor-bearing mice, and MgIG inhibited the abnormal increase caused by oxaliplatin ($p<0.001$, Fig. 2E, F).

MgIG attenuates the expression of Mito-Cx43 in HSCs induced by oxaliplatin

GFAP was used as the marker of HSCs, and the expression of Cx43 and its colocalization with HSCs were determined by immunofluorescence. The results showed that the expression of Cx43 was increased by oxaliplatin, and colocalization with HSCs was observed. Intervention with MgIG inhibited the expression of Cx43 in liver tissue and reduced the colocalization of Cx43 with HSCs (Fig. 3). We stimulated LX-2 cells with 2 μg/mL oxaliplatin and assayed Cx43 by immunofluorescence. The results showed that oxaliplatin induced the expression of Cx43 and its localization in mitochondria in LX-2

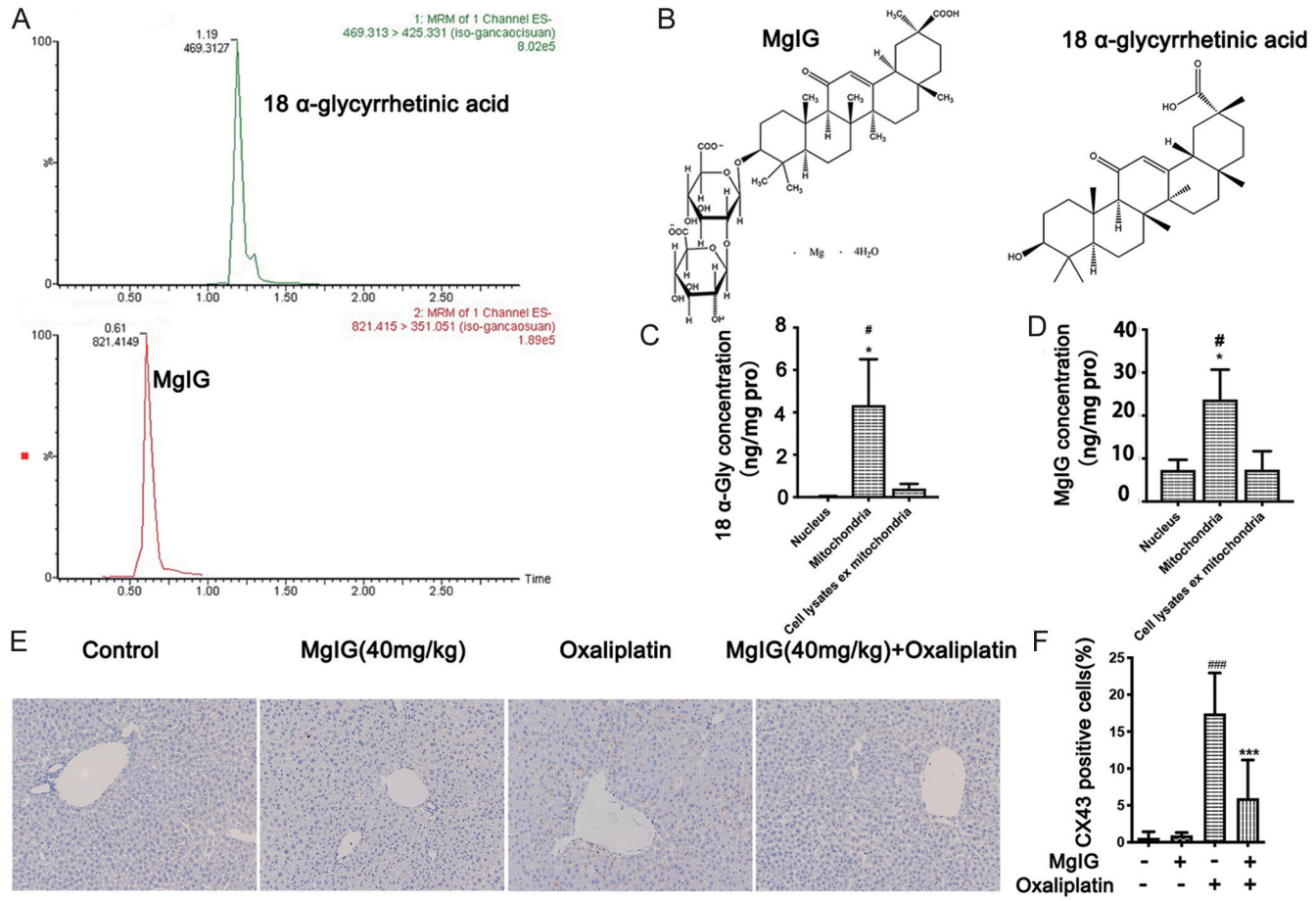

Fig. 2. Distribution of MgIG and the liver injury related protein Cx43 expression in MgIG- or oxaliplatin-treated mice livers. (A) Typical high-performance liquid chromatogram of MgIG and 18-α-glycyrrhetinic acid; (B) The chemical structure of MgIG and 18-α-glycyrrhetinic acid; (C–D) Concentrations of 18-α-glycyrrhetinic acid (C) and MgIG (D) in the liver after administration of MgIG at 40 mg/kg. Compared with nuclei: $^{\#}p<0.05$; Compared with cell lysates ex mitochondria: $^{*}p<0.05$. ($n=3$ in each group). (E, F) Representative immunohistochemical staining (E) and semiquantification (F) of Cx43 in mice liver. (magnification ×200, $n=6$). Compared with untreated group: $^{\#\#\#}p<0.001$; Compared with oxaliplatin-treated group: $^{***}p<0.001$. Cx43, connexin 43; MgIG, magnesium isoglycyrrhizinate.

cells (Fig. 4A). We extracted mitochondria to detect changes in expression of Mito-Cx43 in LX2 cells by western blotting. The results showed that MgIG significantly reduced the level of Cx43 in mitochondria ($p<0.001$, Fig. 4B, C). Oxaliplatin induced Cx43 expression in LX-2 cells and colocalization with the mitochondria marker TOM20. However, when MgIG was given before oxaliplatin, colocalization was reduced. The results indicate that MgIG reversed the increased expression of Cx43 in HSCs caused by oxaliplatin. Oxaliplatin induced Cx43 expression in the cytoplasm, mitochondria, and nuclei. MgIG inhibited the expression of Cx43 (Fig. 4C–E). The inhibitory effects did not rely on translocation of Cx43.

MgIG inhibits oxaliplatin-induced liver fibrosis and lipid deposition

Liver fibrosis and abnormal accumulation of lipids are induced by damage of mitochondria. Collagen deposition and α-SMA expression are recognized markers of liver fibrosis. Collagen deposition in liver tissues was observed by Masson staining, and α-SMA expression was assayed by immunohistochemistry. The results of Masson staining and immunohistochemistry of α-SMA both showed that MgIG had effects on oxaliplatin-induced liver fibrosis (Fig. 5A, B). Oil red O staining also showed that MgIG alleviated oxaliplatin-induced liver lipid deposition (Fig. 5C). The results indicate that MgIG relieved oxaliplatin-induced liver fibrosis. The activation of HSCs is the main cause of liver fibrosis. We determined the protein level of α-SMA by immunofluorescence *in vitro*, finding that the protein level of α-SMA was enhanced in LX-2 cells induced by oxaliplatin (Fig. 5D). The expression of collagen I in LX2 cells was also significantly increased by oxaliplatin ($p<0.001$, Fig. 5E, F). After MgIG intervention, the expression of α-SMA (Fig. 5D) and the expression of collagen I were significantly reduced compared with administration of oxaliplatin alone ($p<0.01$, **, Fig. 5E–F). Oil red O staining also showed that MgIG reduced oxaliplatin-induced lipid deposition in LX-2 cells (Fig. 5G).

MgIG attenuates Mito-Cx43 and activation of HSCs

To further confirm the effect of MgIG on Mito-Cx43 expression in HSCs, LPS was used to activate Cx43 as a positive model control in LX-2 cells. Immunofluorescence staining showed that Cx43 expression was enhanced after LPS treatment compared with the blank group, and colocalization occurred between the green fluorescence-labeled TOM and the red fluorescence-labeled Cx43. Red fluorescence intensity was decreased after the intervention of MgIG, and colocalization of green and red fluorescence was significantly reduced (Fig.

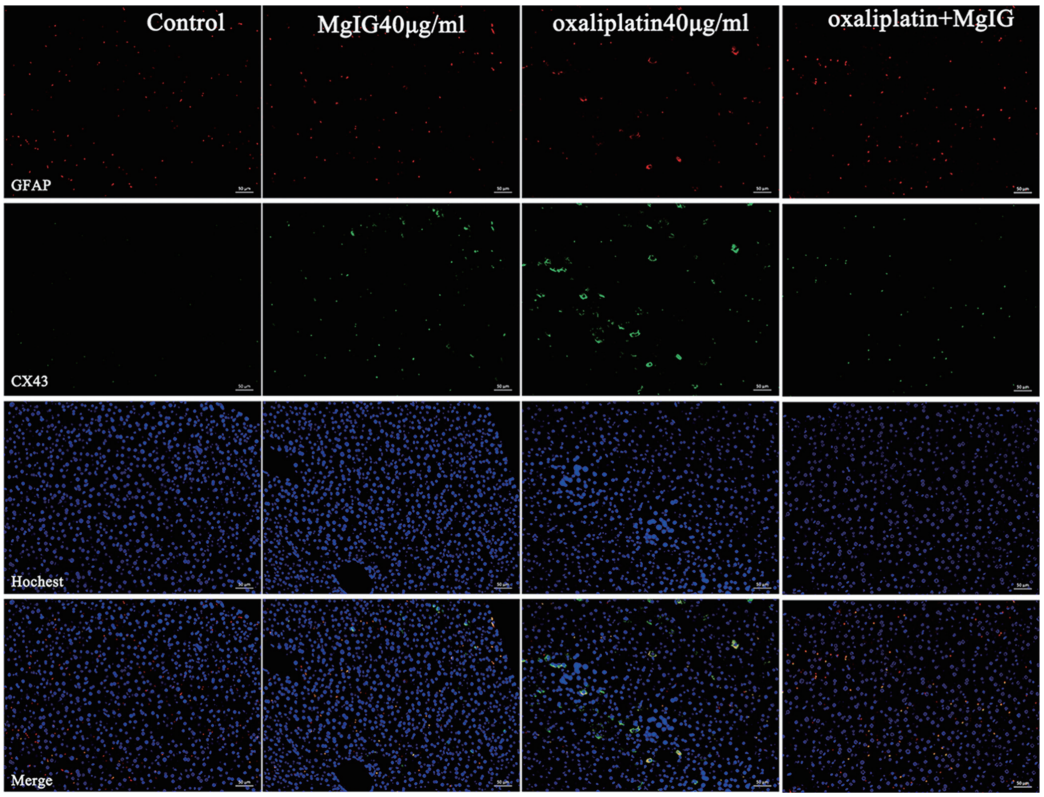

Fig. 3. MgIG (40 mg/kg) inhibited Cx43 expression in activated HSCs induced by oxaliplatin (6 mg/kg) in tumor-bearing mice. Representative immunofluorescence staining of Cx43 and GFAP (HSC activation marker) in mouse liver. Mouse liver sections were stained with anti-GFAP antibody conjugated with Cy3 (red) and anti-Cx43 antibody conjugated with fluorescein isothiocyanate (FITC, green). Nuclei were stained with Hoechst (blue). Arrows indicated the colocalization of the two proteins on merged images (yellow). *n*=3 in each group. Cx43, connexin 43; HSC, hepatic stellate cell; MgIG, magnesium isoglycyrrhizinate.

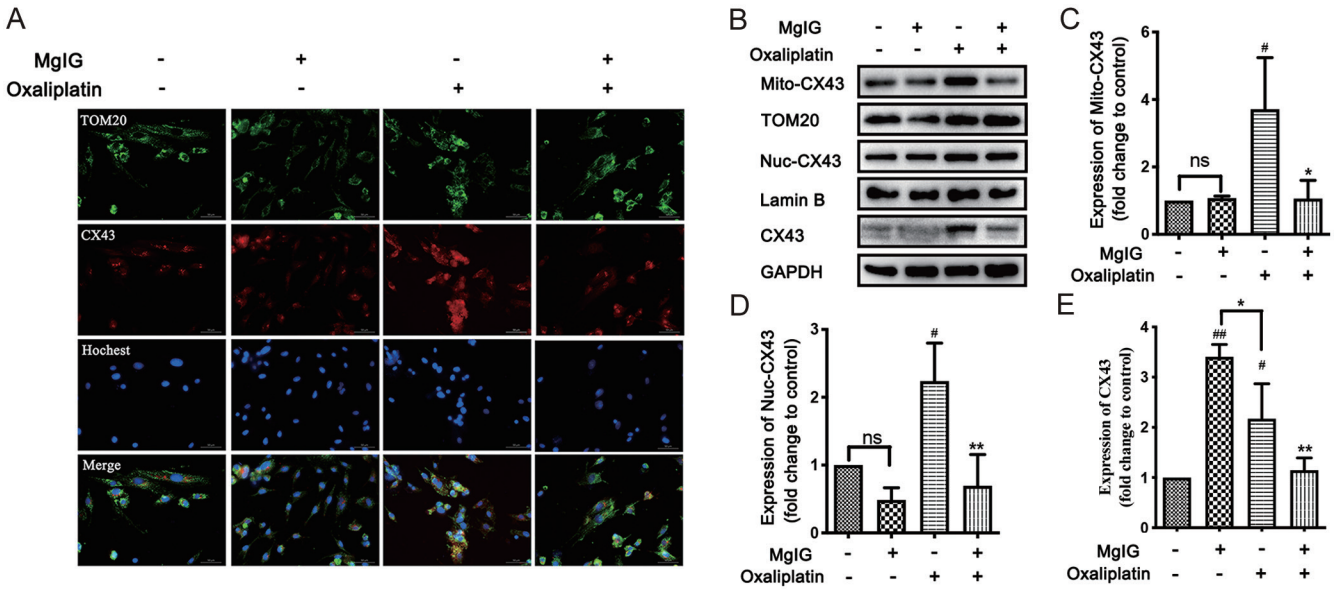

Fig. 4. MgIG (40 μg/mL) inhibited mitochondrial Cx43 expression in HSCs induced by oxaliplatin (2 μg/mL) in LX-2 human HSC cell lines. (A) Immunofluorescent staining of Cx43 and mitochondria marker TOM20 in LX-2 cells. Cells were stained with anti-Cx43 antibody conjugated to Cy3 (red) and anti-TOM20 conjugated to FITC (green). Nuclei were stained with Hoechst (blue). Arrows indicated the colocalization of the two proteins on merged images (yellow). (magnification, ×400 *n*=3) (B) Western blot assays of Cx43 in mitochondria, nuclei, and cytoplasm of LX-2 cells. TOM20, lamin B, and GADPH were the loading controls for mitochondria, nuclei, and cytoplasm protein, respectively. (C–E) Semiquantification of western blot bands in (B) of Cx43 protein expression in mitochondria (C), nuclei (D) and total Cx43 (E). Each column represents a mean ± SD (*n*=3). Compared with untreated group: $^{\#}p<0.05$; Compared with oxaliplatin-treated group: $^{*}p<0.05$. NS, not significant. Cx43, connexin 43; HSC, hepatic stellate cell; MgIG, magnesium isoglycyrrhizinate.

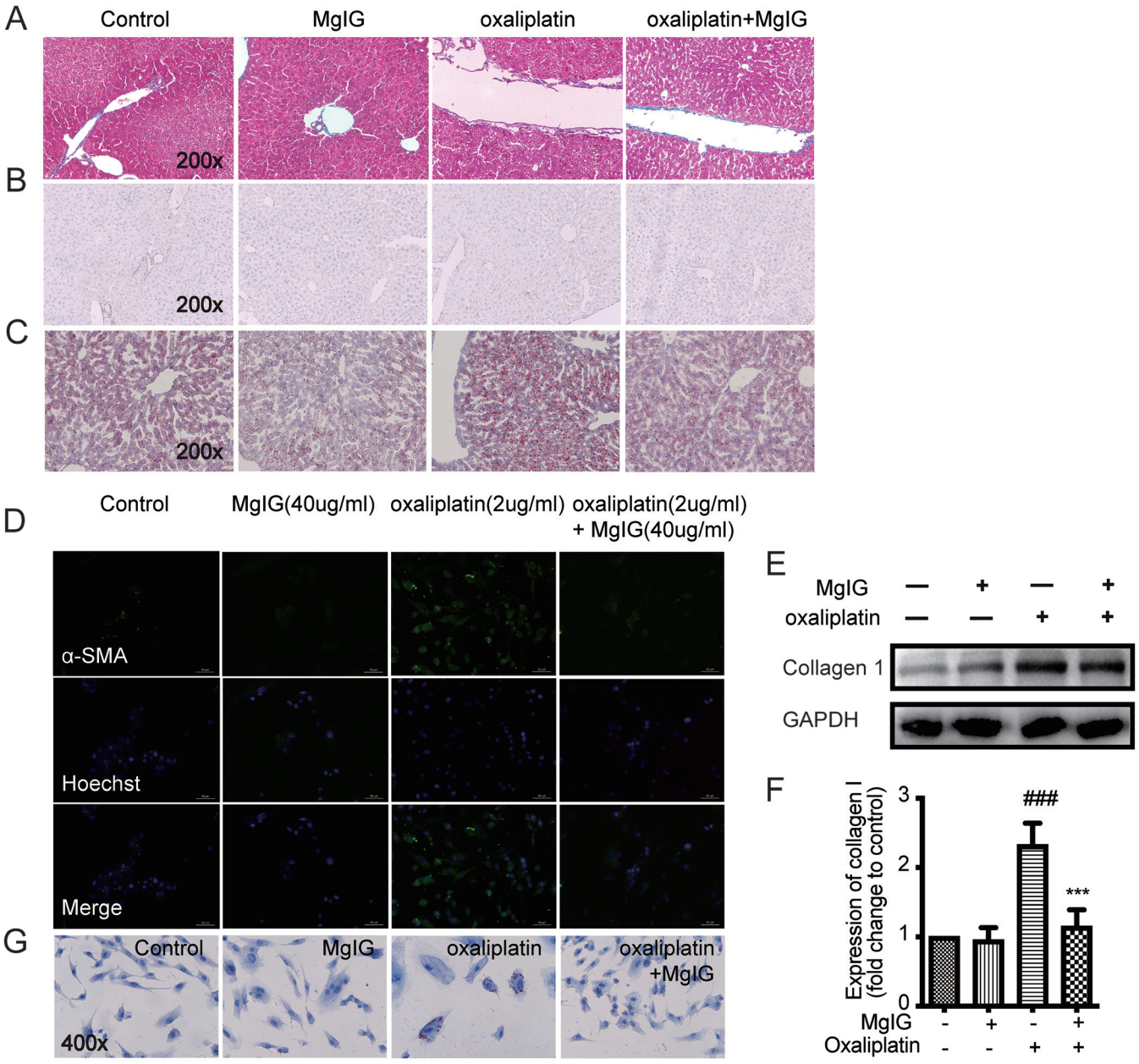

Fig. 5. MgIG inhibited oxaliplatin-induced liver fibrosis and lipid deposition. (A) Representative images of Masson staining of mouse liver tissues (magnification ×200, *n*=3). (B) immunohistochemical staining of α-SMA in mouse liver tissue (magnification ×200, *n*=3). (C) Oil red O staining of mouse liver (magnification ×200, *n*=3). (D) Representative images of immunofluorescence staining of α-SMA in LX-2 cells. Nuclei were stained with Hoechst (blue) (magnification ×200, *n*=3). (E, F) Western blots of collagen I in LX-2 cells. GAPDH was the loading control. Band intensities were quantified with Image J software and plotted in F. Each column represents a mean ± SD (*n*=3). Compared with untreated group: $^{###}p<0.001$; Compared with oxaliplatin-treated group: $^{**}p<0.01$, $^{***}p<0.001$. (G) Representative images of Oil red O staining of lipid droplets in LX-2 cells. (magnification ×200, *n*=3). MgIG, magnesium isoglycyrrhizinate.

6A, E). In addition, MgIG reduced LPS-induced lipid droplet deposition and α-SMA fluorescence expression levels in LX-2 cells (Fig. 6B–D, F). After Cx43 was knocked down in LX-2 cells by lentiviral transduction (Fig. 7A, B). Although oxaliplatin induced lipid deposition in Cx43-depleted LX-2 cells, the inhibitory effect of MgIG on oxaliplatin-induced Cx43-depleted LX-2 cells, lipid deposition and the fluorescence intensity of α-SMA was reduced (Fig. 7C, D, J). Moreover, the inhibition of LPS-induced HSC activation, lipid deposition, and α-SMA expression were attenuated in Cx43-depleted LX-2 cells (Fig. 7D, C–J). The results suggest that Cx43 was involved in the inhibition of oxaliplatin-induced LX-2 activation by MgIG.

MgIG attenuates the activation of HSCs by reducing ROS generation, mitochondria dysfunction, and transcription of N-cadherin

In drug-induced liver injury, mitochondria are highly susceptible to damage that results in dysfunction.[25] An increase of ROS is the main manifestation of mitochondrial dysfunction and is an important factor for inducing HSC activation and

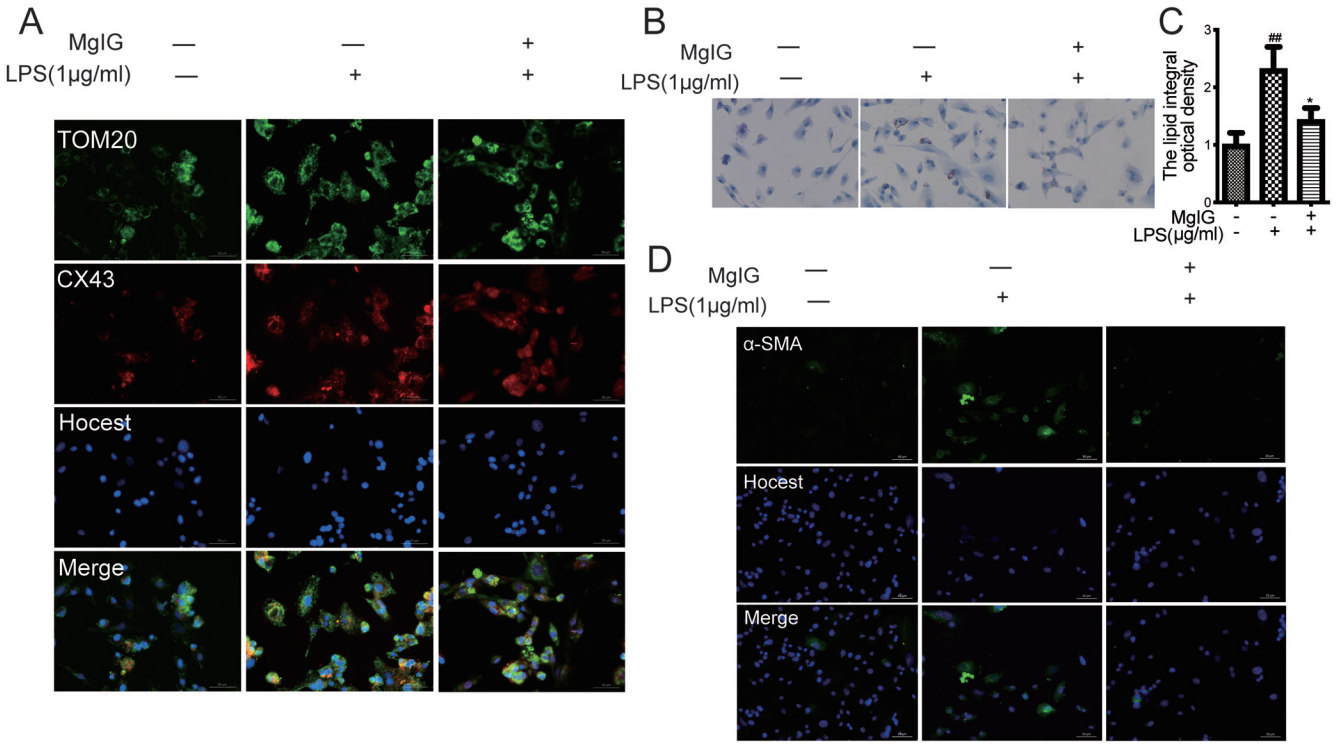

Fig. 6. Effects of MgIG on α-SMA abnormalities and lipid deposition in LPS-treated LX-2 cells. (A) Representative images of immunofluorescence of Cx43 in LX-2 cells. LX-2 was stained for Cx43 with Cy3 (red) and TOM20 with FITC (green). Nuclei were stained with Hoechst (blue) (original magnification ×400, n=3). (B–C) The effect of MgIG on lipid deposition in LX-2 was detected by Oil red O staining. (original magnification ×400, *n*=3).The level of lipid deposition was assessed by measuring absorbance. (D) Representative images of immunofluorescence staining of α-SMA in LX-2. Nuclei were stained with Hoechst (blue) (original magnification ×400, *n*=3). Compared with untreated control: $^{\#\#}p<0.01$; Compared with LPS group: $^{*}p<0.05$. MgIG, magnesium isoglycyrrhizinate.

hepatic fibrosis.[26] In addition, an increase in ROS causes destruction of the mitochondrial membrane potential.[27] The results showed that oxaliplatin exposure induced oxidative stress in LX-2 cells, and that ROS were decreased after intervention of MgIG (Fig. 8A, B). Quantification of JC-1 fluorescence intensity (red/green fluorescence intensity) indicated that MgIG reduced mitochondria dysfunction that was induced by oxaliplatin (Fig. 8C, D) and that the protection of mitochondria by MgIG may be related to reduction of Cx43.[28]

Previous immunofluorescence and western blot data showed that MgIG not only attenuates the level of Cx43 in mitochondria, but also inhibits oxaliplatin-induced Cx43 entry into the nucleus (Fig 4A–D). Because Cx43 has been reported to function as transcription factor to activate N-cadherin,[15] we assayed the expression of the downstream protein N-cadherin by western blotting. The results revealed that oxaliplatin stimulated the expression of N-cadherin in LX-2 cells, while MgIG intervention reduced N-cadherin (Fig. 8E, F). As a key regulator and indicator of HSC activation, N-cadherin drives epithelial-mesenchymal transition (EMT) and inhibits the apoptosis of HSCs.[29,30] The results indicate that MgIG inhibited oxaliplatin-induced HSC activation, which was closely related to its regulation of Cx43 in mitochondria and nuclei.

Discussion

Oxaliplatin is successfully used for management of colorectal cancer and is the standard treatment of metastatic disease. However, it may cause liver injury, particularly sinusoidal obstruction syndrome, which is characterized by histologic changes such as sinusoidal dilatation and congestion, fibrosis, and obstruction. The histopathological changes result from drug-induced damages to endothelial cells and activation of HSCs.[31] Our study focused on HSCs and used *in vitro* and *in vivo* models to investigate the mechanisms of MgIG in protecting liver from oxaliplatin-based chemotherapy. We found that MgIG inhibited oxaliplatin- or LPS-induced HSC activation and collagen and lipid deposition. Gap junction protein alterations are closely related with liver diseases including drug-induced liver toxicity. Cx43 is the major gap junction protein expressed on HSCs. Results of ours and previous studies demonstrated that oxaliplatin induced Cx43 expression in liver cells, which indicates that Cx43 mediated oxaliplatin-induced liver injury.[32] MgIG treatment attenuated Cx43 expression induced by oxaliplatin or LPS in tumor-bearing mice or LX-2 cells. By performing shRNA knockdown experiments, we verified that Cx43 mediated the inhibitory effects of MgIG on HSC activation and lipid deposition induced by oxaliplatin or LPS.

Cx43 is the major gap junction protein in HSCs and mediates liver damage induced by acetaminophen,[33,34] oxaliplatin,[35] cisplatin,[36] cadmium,[37] and sevoflurane.[38] It also has a role in maintaining liver hemostasis. Hepatocyte cell proliferation was reduced and fewer necroinflammatory lesions were present in the liver parenchyma of Cx43 deficient mice (PMID: 20830702). Our study and those of others have shown that Cx43 is highly expressed in HSCs (Fig. 3).[39] The data indicate that Cx43 is a potential target for diseases and pathologies related to activation of HSCs. Inhibition of the gap junction protein may reduce drug toxicity by preventing the propagation of inflammatory or death stimuli to neigh-

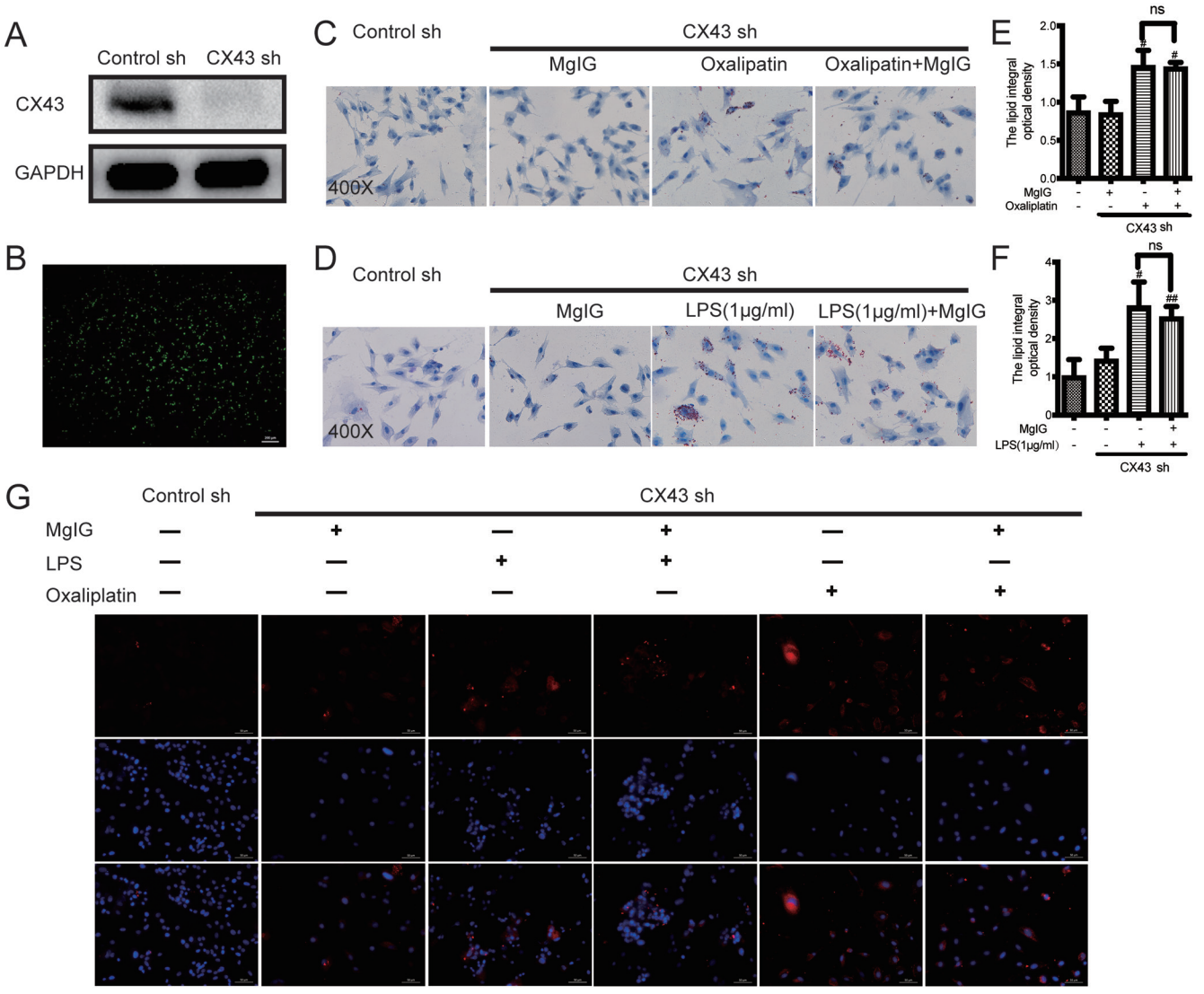

Fig. 7. Effects of Cx43-knockdown on the protective effects of MgIG in oxaliplatin or LPS-induced LX-2 cells. (A) Western blot assay of cell lysates of Cx43 in vector control or Cx43-knockdown LX-2 cells. (B) Fluorescence image of LX-2 cells expressing Cx43-knockdown plasmids. (original magnification ×200). (C–F) Oil red O staining of Cx43-knockdown LX-2 cells and semiquantitative analysis by measuring the absorbance value. Each value represents mean± SD (n=3) Compared with untreated control: $^{\#}p<0.05$; Compared with oxaliplatin or LPS group: $^{*}p<0.05$; NS, not significant. (G) Immunofluorescence staining of α-SMA in Cx43-knockdown LX-2 cells. Nuclei were stained with Hoechst (blue) (n=3). Cx43, connexin 43; MgIG, magnesium isoglycyrrhizinate.

boring cells.[16] Apart from its localization at the cytomembrane and endoplasmic reticulum, Cx43 is also expressed in mitochondria and nuclei. Our current understanding of mitochondrial Cx43 is based on heart disease scenarios. Cx43 translocates into mitochondria and regulates apoptosis and oxidative stress in terms of ROS production, calcium overload, and mitochondrial membrane depolarization in myocardial hypoxia.[40] However, whether mitochondrial Cx43 is involved in hepatotoxicity is unknown. Presently, we found that MgIG reduced the expression level of Cx43 in the mitochondria and nuclei of LX2 cells induced by oxaliplatin (Fig. 4). Besides its functions in mitochondria, Cx43 increased the transcriptional regulation of N-cadherin.[15] As an important regulator of HSC activation, N-cadherin promotes EMT and inhibits the apoptosis of HSCs.[41,42] We showed that oxaliplatin stimulated the expression of N-cadherin in HSCs, while MgIG intervention reduced N-cadherin (Fig. 8). Cx43 has a critical role in drug-induced organ injury, especially in the liver, kidney, and gastrointestinal tract.[35] Therefore, the clinical implications of our study may be related to increased susceptibility to drug-induced organ injury.

The study has some limitations. We did not provide direct evidence of the binding of MgIG to Cx43 protein. Several reports have described the use of 18 α-glycyrrhetinic acid to block intercellular communication and inhibit the expression of Cx43.[43–45] We found that MgIG and its metabolite 18 α-glycyrrhetinic acid could be detected in mitochondria *in vivo* (Fig. 2A–C). It might be possible confirm the direct binding of MgIG or 18 α-glycyrrhetinic acid to Cx43 in mitochondria by microscale thermophoresis.

In China, MgIG has been used in combination with oxaliplatin to treat tumors, but the mechanism of MgIG protection against liver injury induced by oxaliplatin and its effect on tumors has not been elucidated. Our study shows that MgIG

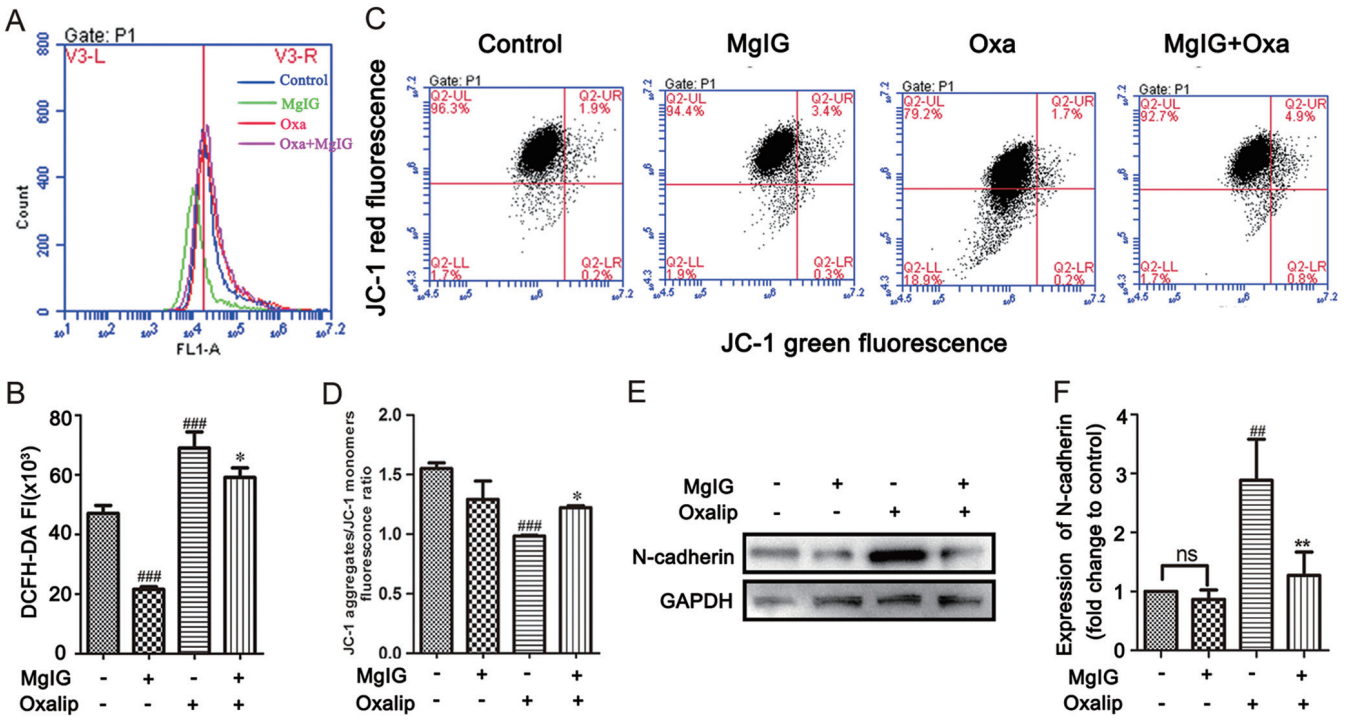

Fig. 8. MgIG attenuated the activation of HSCs. (A, B) Flow cytometry of reactive oxygen species (ROS) generation. ROS level is expressed as the DCFH-DA fluorescence intensity, each value represents a mean ± SD (n=3); (C) Measurement of mitochondrial membrane potential visualized by JC-1. (D) Quantification of JC-1 fluorescence intensity (red/green), each value represents a mean ± SD (n=3); (E, F) Western blot assays of N-cadherin in LX-2 cells. Each column represents a mean ± SD (n=3). (G) Schematic summary of the suggested role of MgIG in oxaliplatin-induced liver injury. Compared with untreated control: $^{\#\#}p<0.01$, $^{\#\#\#}p<0.001$; Compared with oxaliplatin group: $^{*}p<0.05$, $^{**}p<0.01$; NS, not significant. HSC, hepatic stellate cell; MgIG, magnesium isoglycyrrhizinate.

was hepatoprotective against oxaliplatin-induced liver injury in tumor-bearing mice, and did not affect the therapeutic effectiveness of oxaliplatin against tumors and Cx43 mediated the protection of MgIG against liver injury. Our study may shed some light on the clinical application of MgIG for patients with Cx43-disturbed expression under pathological conditions.

Acknowledgments

The authors thank Nanjing Jiangbei New Area Biopharmaceutical Public Service Platform for assisting the project.

Funding

This project was supported by the Open Project Program of Jiangsu Key Laboratory for Pharmacology and Safety Evaluation of Chinese Materia Medica (No. JKLPSE201501), the Open Project of Chinese Materia Medica First-Class Discipline of Nanjing University of Chinese Medicine (No. 2020YLXK20), and the Science and Technology Development Foundation of Nanjing Medical University (No. NMUB2019186).

Conflict of interest

The authors have no conflict of interests related to this publication.

Author contributions

Performance of the experiments (YC, HS, YW), analysis of the data and generation of the figures (YC. YX), design of the project and writing of the paper (YX, YW, YL).

Ethical statement

The study procedures were approved by the Institutional Animal Care and Use Committee of Nanjing University of Chinese Medicine (Nanjing, China; Approval No. ACU170905).

Data sharing statement

The data used and analyzed in this study are available from the corresponding authors, upon reasonable request.

References

[1] Grothey A, Fakih M, Tabernero J. Management of BRAF-mutant metastatic colorectal cancer: a review of treatment options and evidence-based guidelines. Ann Oncol 2021;32(8):959–967. doi:10.1016/j.annonc.2021.03.206, PMID:33836264.
[2] Naiki-Ito A, Asamoto M, Naiki T, Ogawa K, Takahashi S, Sato S, *et al*. Gap junction dysfunction reduces acetaminophen hepatotoxicity with impact on apoptotic signaling and connexin 43 protein induction in rat. Toxicol Pathol 2010;38(2):280–286. doi:10.1177/0192623309357951, PMID:20097795.
[3] Rubbia-Brandt L, Audard V, Sartoretti P, Roth AD, Brezault C, Le Charpentier M, *et al*. Severe hepatic sinusoidal obstruction associated with oxaliplatin-based chemotherapy in patients with metastatic colorectal cancer. Ann Oncol 2004;15(3):460–466. doi:10.1093/annonc/mdh095, PMID:14998849.
[4] Liao X, Bu Y, Chang F, Jia F, Song G, Xiao X, *et al*. Remodeling of hepatic stellate cells orchestrated the stroma-derived oxaliplatin-resistance through CCN3 paracrine in hepatocellular carcinoma. BMC Cancer 2019;19(1):1192. doi:10.1186/s12885-019-6362-1, PMID:31805888.
[5] Stevenson HL, Prats MM, Sasatomi E. Chemotherapy-induced Sinusoidal Injury (CSI) score: a novel histologic assessment of chemotherapy-related hepatic sinusoidal injury in patients with colorectal liver metastasis. BMC Cancer 2017;17(1):35. doi:10.1186/s12885-016-2998-2, PMID:28061766.
[6] Tajima H, Ohta T, Miyashita T, Nakanuma S, Matoba M, Miyata T, *et al*. Ox-

aliplatin-based chemotherapy induces extravasated platelet aggregation in the liver. Mol Clin Oncol 2015;3(3):555–558. doi:10.3892/mco.2015.512, PMID:26137266.
[7] Jinghui H, dongshan Y, Xin C, Yuna Z, Aimin C. Protective effect of magnesium isoglycyrrhizinate on liver function in patients with gastrointestinal cancer chemotherapy. International journal of experimental medicine 2017;38(11):1485–1487.
[8] Tang GH, Yang HY, Zhang JC, Ren JJ, Sang XT, Lu X, *et al*. Magnesium isoglycyrrhizinate inhibits inflammatory response through STAT3 pathway to protect remnant liver function. World J Gastroenterol 2015;21(43):12370–12380. doi:10.3748/wjg.v21.i43.12370, PMID:26604644.
[9] He M, Li Q, Zou R, Shen J, Fang W, Tan G, *et al*. Sorafenib Plus Hepatic Arterial Infusion of Oxaliplatin, Fluorouracil, and Leucovorin vs Sorafenib Alone for Hepatocellular Carcinoma With Portal Vein Invasion: A Randomized Clinical Trial. JAMA Oncol 2019;5(7):953–960. doi:10.1001/jamaoncol.2019.0250, PMID:31070690.
[10] Zou X, Wang Y, Peng C, Wang B, Niu Z, Li Z, *et al*. Magnesium isoglycyrrhizinate has hepatoprotective effects in an oxaliplatin-induced model of liver injury. Int J Mol Med 2018;42(4):2020–2030. doi:10.3892/ijmm.2018.3787, PMID:30066834.
[11] Xianju W. Therapeutic effect of magnesium isoglycyrrhizinate on liver injury induced by oxaliplatin. Chinese Practical Medicine 2016;11(01):140–141.
[12] Sun L, Shen J, Pang X, Lu L, Mao Y, Zeng M. Phase I safety and pharmacokinetic study of magnesium isoglycyrrhizinate after single and multiple intravenous doses in chinese healthy volunteers. J Clin Pharmacol 2007;47(6):767–773. doi:10.1177/0091270007299757, PMID:17409184.
[13] Yang Q, Wang J, Liu R, Wang Z, Li Y, Zhang Y, *et al*. Amelioration of concanavalin A-induced autoimmune hepatitis by magnesium isoglycyrrhizinate through inhibition of CD4(+)CD25(-)CD69(+) subset proliferation. Drug Des Devel Ther 2016;10:443–453. doi:10.2147/DDDT.S92440, PMID:26869766.
[14] Jiang W, Chen Q, Li P, Lu Q, Pei X, Sun Y, *et al*. Magnesium Isoglycyrrhizinate attenuates lipopolysaccharide-induced depressive-like behavior in mice. Biomed Pharmacother 2017;86:177–184. doi:10.1016/j.biopha.2016.12.033, PMID:27978497.
[15] Kotini M, Barriga EH, Leslie J, Gentzel M, Rauschenberger V, Schambony A, *et al*. Gap junction protein Connexin-43 is a direct transcriptional regulator of N-cadherin in vivo. Nat Commun 2018;9(1):3846. doi:10.1038/s41467-018-06368-x, PMID:30242148.
[16] Balasubramaniyan V, Dhar DK, Warner AE, Vivien Li WY, Amiri AF, Bright B, *et al*. Importance of Connexin-43 based gap junction in cirrhosis and acute-on-chronic liver failure. J Hepatol 2013;58(6):1194–1200. doi:10.1016/j.jhep.2013.01.023, PMID:23376361.
[17] Wang Q, You T, Yuan D, Han X, Hong X, He B, *et al*. Cisplatin and oxaliplatin inhibit gap junctional communication by direct action and by reduction of connexin expression, thereby counteracting cytotoxic efficacy. J Pharmacol Exp Ther 2010;333(3):903–911. doi:10.1124/jpet.109.165274, PMID:20215407.
[18] Zou ZW, Chen HJ, Yu JL, Huang ZH, Fang S, Lin XH. Gap junction composed of connexin43 modulates 5-fluorouracil, oxaliplatin and irinotecan resistance on colorectal cancers. Mol Med Rep 2016;14(5):4893–4900. doi:10.3892/mmr.2016.5812, PMID:27748862.
[19] Gonzalez-Aparicio M, Alzuguren P, Mauleon I, Medina-Echeverz J, Hervas-Stubbs S, Mancheno U, *et al*. Oxaliplatin in combination with liver-specific expression of interleukin 12 reduces the immunosuppressive microenvironment of tumours and eradicates metastatic colorectal cancer in mice. Gut 2011;60(3):341–349. doi:10.1136/gut.2010.211722, PMID:20855451.
[20] Hu Q, Ding J, Liu S, Li P, Hu G. Pharmacokinetics of magnesium glycyrrhizinate following intravenous administration of magnesium glycyrrhizinate in rats. Eur J Drug Metab Pharmacokinet 2003;28(4):259–264. doi:10.1007/BF03220177, PMID:14743966.
[21] Wang Y, Zhang Z, Wang X, Qi D, Qu A, Wang G. Amelioration of Ethanol-Induced Hepatitis by Magnesium Isoglycyrrhizinate through Inhibition of Neutrophil Cell Infiltration and Oxidative Damage. Mediators Inflamm 2017;2017:3526903. doi:10.1155/2017/3526903, PMID:28951632.
[22] Chen P, Luo Q, Huang C, Gao Q, Li L, Chen J, *et al*. Pathogenesis of non-alcoholic fatty liver disease mediated by YAP. Hepatol Int 2018;12(1):26–36. doi:10.1007/s12072-017-9841-y, PMID:29330836.
[23] Kleiner DE, Brunt EM, Van Natta M, Behling C, Contos MJ, Cummings OW, *et al*. Design and validation of a histological scoring system for nonalcoholic fatty liver disease. Hepatology 2005;41(6):1313–1321. doi:10.1002/hep.20701, PMID:15915461.
[24] Won DH, Hwang DB, Shin YS, Kim SY, Kim C, Hong IS, *et al*. Cellular signaling crosstalk between Wnt signaling and gap junctions inbenzo[a]pyrene toxicity. Cell Biol Toxicol 2021. doi:10.1007/s10565-021-09630-z, PMID:34283317.
[25] Chen Z, Lu X, McGee-Lawrence ME, Watsky MA. Transient Cell Membrane Disruptions induce Calcium Waves in Corneal Keratocytes. Sci Rep 2020;10(1):2840. doi:10.1038/s41598-020-59570-7, PMID:32071321.
[26] Bertero E, Nickel A, Kohlhaas M, Hohl M, Sequeira V, Brune C, *et al*. Loss of Mitochondrial Ca2+ Uniporter Limits Inotropic Reserve and Provides Trigger and Substrate for Arrhythmias in Barth Syndrome Cardiomyopathy. Circulation 2021;144(21):1694–1713. doi:10.1161/CIRCULATIONAHA.121.053755, PMID:34648376.
[27] Jia Z, Yuan X, Wei JA, Guo X, Gong Y, Li J, *et al*. A Functionalized Octahedral Palladium Nanozyme as a Radical Scavenger for Ameliorating Alzheimer's Disease. ACS Appl Mater Interfaces 2021;13(42):49602–49613. doi:10.1021/acsami.1c06687, PMID:34641674.
[28] Ruiz-Meana M, Rodríguez-Sinovas A, Cabestrero A, Boengler K, Heusch G, Garcia-Dorado D. Mitochondrial connexin43 as a new player in the pathophysiology of myocardial ischaemia-reperfusion injury. Cardiovasc Res 2008;77(2):325–333. doi:10.1093/cvr/cvm062, PMID:18006437.
[29] Giannelli G, Koudelkova P, Dituri F, Mikulits W. Role of epithelial to mesenchymal transition in hepatocellular carcinoma. J Hepatol 2016;65(4):798–808. doi:10.1016/j.jhep.2016.05.007, PMID:27212245.
[30] Sun YL, Bai T, Zhou L, Zhu RT, Wang WJ, Liang RP, *et al*. SOD3 deficiency induces liver fibrosis by promoting hepatic stellate cell activation and epithelial-mesenchymal transition. J Cell Physiol 2021;236(6):4313–4329. doi:10.1002/jcp.30174, PMID:33230845.
[31] Choi JH, Won YW, Kim HS, Oh YH, Lim S, Kim HJ. Oxaliplatin-induced sinusoidal obstruction syndrome mimicking metastatic colon cancer in the liver. Oncol Lett 2016;11(4):2861–2864. doi:10.3892/ol.2016.4286, PMID:27073565.
[32] Hernández-Guerra M, Hadjihambi A, Jalan R. Gap junctions in liver disease: Implications for pathogenesis and therapy. J Hepatol 2019;70(4):759–772. doi:10.1016/j.jhep.2018.12.023, PMID:30599172.
[33] Jung SH, Lee W, Park SH, Lee KY, Choi YJ, Choi S, *et al*. Diclofenac impairs autophagic flux via oxidative stress and lysosomal dysfunction: Implications for hepatotoxicity. Redox Biol 2020;37:101751. doi:10.1016/j.redox.2020.101751, PMID:33080439.
[34] Maes M, Crespo Yanguas S, Willebrords J, Weemhoff JL, da Silva TC, Decrock E, *et al*. Connexin hemichannel inhibition reduces acetaminophen-induced liver injury in mice. Toxicol Lett 2017;278:30–37. doi:10.1016/j.toxlet.2017.07.007, PMID:28687253.
[35] Katturajan R, Evan Prince S. A role of connexin 43 on the drug-induced liver, kidney, and gastrointestinal tract toxicity with associated signaling pathways. Life Sci 2021;280:119629. doi:10.1016/j.lfs.2021.119629, PMID:34004253.
[36] Kim YJ, Kim J, Kim YS, Shin B, Choo OS, Lee JJ, *et al*. Connexin 43 Acts as a Proapoptotic Modulator in Cisplatin-Induced Auditory Cell Death. Antioxid Redox Signal 2016;25(11):623–636. doi:10.1089/ars.2015.6412, PMID:27122099.
[37] Zou H, Zhuo L, Han T, Hu D, Yang X, Wang Y, *et al*. Autophagy and gap junctional intercellular communication inhibition are involved in cadmium-induced apoptosis in rat liver cells. Biochem Biophys Res Commun 2015;459(4):713–719. doi:10.1016/j.bbrc.2015.03.027, PMID:25778869.
[38] Huang F, Li S, Gan X, Wang R, Chen Z. Propofol inhibits gap junctions by attenuating sevoflurane-induced cytotoxicity against rat liver cells in vitro. Eur J Anaesthesiol 2014;31(4):219–224. doi:10.1097/01.EJA.0000435059.98170.da, PMID:24145807.
[39] Fischer R, Reinehr R, Lu TP, Schönicke A, Warskulat U, Dienes HP, *et al*. Intercellular communication via gap junctions in activated rat hepatic stellate cells. Gastroenterology 2005;128(2):433–448. doi:10.1053/j.gastro.2004.11.065, PMID:15685554.
[40] Pecoraro M, Pinto A, Popolo A. Inhibition of Connexin 43 translocation on mitochondria accelerates CoCl2-induced apoptotic response in a chemical model of hypoxia. Toxicol In Vitro 2018;47:120–128. doi:10.1016/j.tiv.2017.11.004, PMID:29155206.
[41] Urushima H, Yuasa H, Matsubara T, Kuroda N, Hara Y, Inoue K, *et al*. Activation of Hepatic Stellate Cells Requires Dissociation of E-Cadherin-Containing Adherens Junctions with Hepatocytes. Am J Pathol 2021;191(3):438–453. doi:10.1016/j.ajpath.2020.12.007, PMID:33345995.
[42] Hartland SN, Murphy F, Aucott RL, Abergel A, Zhou X, Waung J, *et al*. Active matrix metalloproteinase-2 promotes apoptosis of hepatic stellate cells via the cleavage of cellular N-cadherin. Liver Int 2009;29(7):966–978. doi:10.1111/j.1478-3231.2009.02070.x, PMID:19580633.
[43] Davidson JS, Baumgarten IM, Harley EH. Reversible inhibition of intercellular junctional communication by glycyrrhetinic acid. Biochem Biophys Res Commun 1986;134(1):29–36. doi:10.1016/0006-291x(86)90522-x, PMID:3947327.
[44] Davidson JS, Baumgarten IM. Glycyrrhetinic acid derivatives: a novel class of inhibitors of gap-junctional intercellular communication. Structure-activity relationships. J Pharmacol Exp Ther 1988;246(3):1104–1107. PMID:3418512.
[45] Goldberg GS, Moreno AP, Bechberger JF, Hearn SS, Shivers RR, MacPhee DJ, *et al*. Evidence that disruption of connexon particle arrangements in gap junction plaques is associated with inhibition of gap junctional communication by a glycyrrhetinic acid derivative. Exp Cell Res 1996;222(1):48–53. doi:10.1006/excr.1996.0006, PMID:8549672.